Journal of the Korean Physical Society, Vol. 76, No. 11, June 2020, pp. 985∼990

Ripples, Wrinkles, and Crumples in Folded Graphene

You-Shin No,* Ji Hye Lee,* Bae Ho Park and Jin Sik Choi†
Department of Physics, Konkuk University, Seoul 05029, Korea

(Received 4 May 2020; accepted 5 May 2020)

Separation of two-dimensional thin-film-materials into single layers had been considered very challenging both theoretically and experimentally until the mechanical exfoliation method was discovered. After the successful separation of single- and/or few-layer graphene, the possibility of wrinkle formation has been one of the main open topics because they were not readily observed in experiments. Here, we report experimental observations of different kinds of repetitive nanoscale deformations (ripples, wrinkles, and crumples) in folded single-layer graphene (SLG) on an SiO_2 substrate. Using high-vacuum atomic force microscopy, we observed that SLG that was pre-transferred onto an SiO_2 substrate was accidentally folded multiple times during the tip-scanning, resulting in the formation of bilayer and trilayer graphene (TLG). Through high-resolution tapping-mode scanning, we could observe the wrinkles, ripples, and crumples in TLG. Additionally, we observed a herringbone pattern that was attributed to an intermediate stage between the wrinkles and ripples; this intermediate state was labeled as wrinklon structure. In our analysis, to characterize the ripples, wrinkles, and crumples, we measured the spatial repetition and amplitude of each pattern using their average line profile and compared them.

PACS numbers: 62.20.F, 68.03.Cd, 62.20.Qp
Keywords: Graphene, Folding, Ripple, Wrinkle, Crumple, AFM, Friction anisotropy, Crystal orientation
DOI: 10.3938/jkps.76.985

I. INTRODUCTION

Periodic structures such as wrinkles, ripples, and crumples are one of the fascinating features of two-dimensional (2D) materials. Wrinkling is a phenomenon commonly observed in our daily lives. When spreading out a wide cloth on a table, it hardly lays flat without wrinkles, owing to the complexity of the in-plane and out-of-plane strains. Theoretically, according to the Mermin-Wagner theorem, the long-range order of 2D crystals is destroyed by long-wavelength fluctuations [10]. However, the out-of-plane thermal fluctuations of 2D membranes could be suppressed owing to the co-existing in-plane shear deformations, that is, though 2D membranes could exist in 3D space, they had to be wrinkled [11, 12]. The debate on their structural stability continued until graphene, the first 2D crystal to be demonstrated, was isolated by mechanical exfoliation in 2004 [13]. The existence of an ideal 2D crystal with perfect periodicity and flatness in the free state was controversial because a single-atomic layer with long-range crystalline order was considered to be unstable. Moreover, although graphene is a solid-like 2D crystal, its ability to bend and form ripples similar to that of soft condensed matter membranes was surprising. However, Meyer *et al.* revealed through transmission electron microscopy measurements that suspended graphene is not perfectly flat, having out-of-plane deformations [15]. Fasolino *et al.* explained that the cause of the ripples is an uneven mixture of long and short carbon-carbon bonds [16].

Graphene is a single layer of honeycomb-structured carbon atoms, and its excellent electrical properties, especially its massless, relativistic particle-like charge carrier behavior, is caused by its 2D crystal periodicity [14]. However, the presence of wrinkles or ripples in the structure of graphene can modify its electronic properties, thus deteriorating them [17]. Theoretically, the intrinsic thermal fluctuations and interatomic interactions can give rise to a ripple structure in free-standing graphene. Experimentally, the uneven strain distribution formed between graphene and its substrate in the transfer process during mechanical exfoliation and the nonuniform interlayer interactions are suspected to be the cause of the ripples. We previously reported the anisotropic puckering of exfoliated monolayer graphene, which might arise from anisotropic ripple distortions [18]. We could identify the existence of the ripple structure by anisotropic friction signal. However, we would not obtain topographical evidence because the height of the ripple was lower than the height resolution limit of contact-mode atomic force microscopy (AFM). In this paper, we demonstrate wrinkle formation on folded graphene

*These authors contributed equally to this work.
†E-mail: jinschoi@konkuk.ac.kr

using high-resolution dynamic force microscopy (DFM) mode of AFM. Ripples were not observed on single (SLG) and bilayer graphene (BLG) and were only found in folded trilayer regions. We could confirm the presence of wrinkles near the folding edge, ripples far from this, and crumples interconnected to intermediate wrinkle-ripple structures (labeled wrinklons) on trilayer graphene (TLG). Furthermore, we estimate the strain and interlayer interaction of graphene from the amplitude and wavelength of the wrinkles and ripples.

II. EXPERIMENTAL PROCEDURE

SLG was prepared by mechanical exfoliation and folded by repetitive scanning with the AFM cantilever tip. To obtain the topography and the AFM cantilever torsion images simultaneously, we used a friction-signal-sensitive cantilever (PPP-LFMR, NANOSENSORS, Germany) in the constant force mode (1 nN). The cantilever is designed to be extremely soft, having a constant force of ∼0.2 N/m, thickness of ∼1 μm, length of 225 μm, and resonance frequency of ∼23 kHz. Additionally, we used a specific high-resolution cantilever equipped with diamond-like carbon (DLC) tips (NSG01_DLC, NT-MDT, Russia) with a typical curvature radius of 1 nm.

III. RESULTS AND DISCUSSION

Figures 1(a) and (b) show AFM topographic images of graphene before and after folding, respectively. Figure 1(a) shows the pristine state of the SLG, which displays a folded area in the bottom-right region (monolayer-trilayer). However, after repetitive scans, the left side of the SLG edges was torn and folded to form BLG and TLG regions simultaneously. Figure 1(c) schematically illustrates how BLG and TLG are constructed during AFM scanning.

Tearing and folding occurs in most AFM experiments on exfoliated 2D materials, though it is not easy to control the folding size and angle. The cause of the tearing and folding can be that the cantilever tip is contaminated by sticky residues that remained on the substrate after mechanical exfoliation, or that small flakes were torn and attached to the cantilever tip during edge scanning. The contaminants may lift 2D materials when the contaminated tip proceeds across their edges [1]. Alternatively, the cutting and folding could be controlled using an increased loading force [2]. However, the size of the folded region is limited to several micrometers. In the case of SLG grown by chemical vapor deposition (CVD), Wang *et al.* developed a twist-angle-controlled self-folding during transfer onto a substrate to fabricate macroscopic folded BLG on the millimeter scale [3].

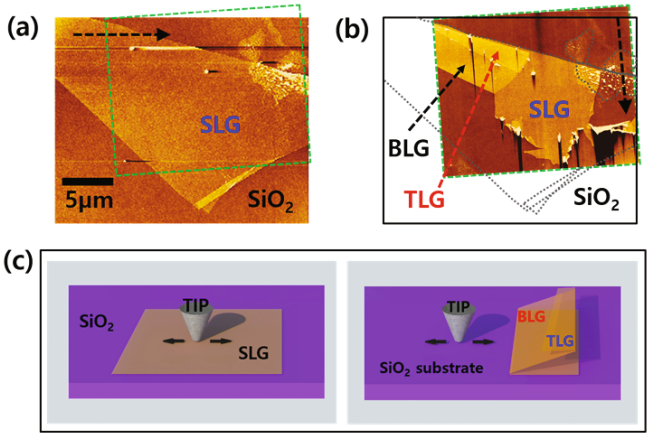

Fig. 1. AFM scan induced-folding of exfoliated SLG on SiO2. AFM topography of exfoliated SLG (a) before and (b) after AFM scanning induced-folding in high vacuum. SLG, BLG, and TLG are colored in blue, black, and red, respectively. A black dotted arrow indicates the fast-scan direction. Because the sample loading directions are different, green dotted rectangles and gray lines are used to match the position of the graphene sample between before and after folding. (c) Schematic diagram of the folding of SLG using AFM, resulting in BLG and TLG.

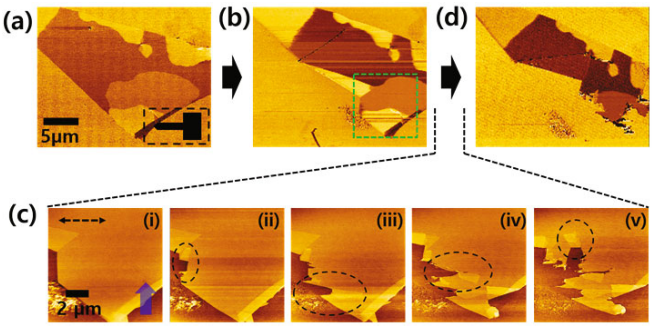

Fig. 2. Graphene shape changes during repetitive scans on SLG. (a), (b), and (d) are cantilever torsion images while scanning longitudinal to the cantilever arm (T_{LON}). (c) AFM topography changes while scanning in the area indicated by a green dotted square in (b). The black dotted arrow indicates the fast-scan direction in T_{LON} and topographic images. The blue arrow in (c-i) shows the slow-scan direction in topography images. The inset in (a) shows the cantilever loading direction for (a), (b), and (d). (a) is obtained at ambient pressure, and (b)–(d) are acquired in high-vacuum conditions ($\sim 10^{-5}$ Torr).

The deposition mechanism of SLG flakes onto a substrate using mechanical exfoliation with a sticky tape has not been revealed. It is not imaginable that graphene remains monolayer on the target substrate. In fact, if SLG is isolated on the sticky tape, it cannot be transferred to the substrate through van der Waals mediated interaction [5] because the adhesion force between the SLG and sticky tape is much higher. Nagashio *et al.* showed that various modified surface structures could affect the

graphene/SiO_2 interaction as well as the electrical properties of graphene [4]. If SLG is mechanically exfoliated, it may suffer complex stress during the transfer from multilayer graphite to a substrate, and chemical interactions may affect its stability. To weaken the chemical interactions between graphene and the substrate, we carried out our AFM experiments in high vacuum ($\sim 10^{-5}$ Torr) maintained by a turbo molecular pump. As expected, SLG could be sequentially folded without increasing the loading force, as shown in Figs. 2(a), (b) and (d). Additionally, we tried to fold another region and compare the tearing and folding behaviors by comparing Figs. 2(b) and (d). During frequent scans, we found that the folding occurs abruptly when the tip crosses an edge.

The tearing and folding behaviors are classified into three types according to the relative folding-scan direction. Though in all cases the cantilever moves at a constant speed in the scan direction, the force applied, such that the tip attached to it may stay at one point, becomes stronger; then, the edge can be torn and folded. (1) The folding direction is oblique to the scan direction. In this case, the resulting tearing and folding areas were larger than those of other folding types [1]. (2) The folding direction is perpendicular to the scan direction, as is the case in Figs. 2(c-ii) and (c-v). We think that, though a greater force than that of (1) was required to tear the edges, it was not applied for a long time because of the vertical scan direction. In this case, the folding area is smaller and multi-folding (*i.e.*, BLG and TLG) occurs. Annett *et al.* controlled such folding by using nanoindentation to fabricate graphene ribbons [6]. (3) In Figs. 2(c-iii) and (c-iv), the interlayer interaction may be stronger than that in (2); therefore, graphene is scratched, and the folding direction is parallel to the scan direction. This phenomenon has been commonly observed in nanoindentation experiments using a high loading force.

Additionally, we investigated friction domain patterns in our exfoliated graphene. Previously, we have categorized the cantilever torsion signals according to the scan direction, relative to the cantilever body direction. Briefly, in normal friction force microscopy (FFM) mode scans, in which the scan direction is perpendicular to the cantilever body direction, the friction can be measured by sensing the cantilever torsion signal. In this mode, we can simultaneously obtain topography information from the parallel bending signals and friction information from the perpendicular torsion signals (torsion signal in the lateral scan, T_{LAT}). However, in the case of anisotropic friction domains, the torsion signals acquired while scanning parallel to the cantilever body direction (torsion signal in the longitudinal scan, T_{LON}) provide more information on the mechanical properties of graphene [7]. This non-destructive friction analysis of exfoliated graphene can be used to identify the crystallographic orientation of graphene and the strain distributions [8, 9]. In the current experiments, we used T_{LON} to investigate the crystal orientation of graphene.

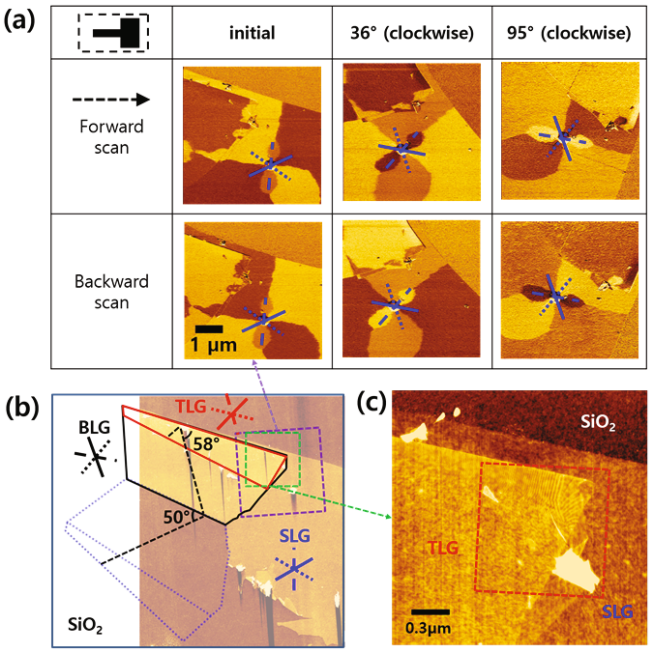

Fig. 3. Crystal orientation of SLG, BLG, and TLG determined through the cantilever torsions resulting from the T_{LON} forward and backward scans. (a) T_{LON} images when the sample is rotated clockwise by 0°, 36°, and 95°. The three overlapped blue radial lines (solid, dotted, broken) represent the zigzag directions of SLG. The ripple directions are determined using the radial ripple domain pattern analysis of the radial stress imposed by an external particle (Fig. 4 in Ref. 9) and confirmed using the sample rotations. (b) Crystal orientation analysis of BLG and TLG by tracking the crystal orientation of the initial SLG and folded graphene and considering the folding angles. The overlapped blue, black, and red radial lines show the zigzag directions of SLG, BLG, and TLG, respectively. (c) High-resolution topographic image obtained using the DFM mode in the green dotted square in (b).

Figures 2(a), (b), and (d) exhibit the friction domain distributions in the SLG and folded BLG regions. Interestingly, the folded region has anisotropic friction domains, similar to that of SLG, and the torsion values change with the relative scan direction.

Through the high-vacuum experiments, large-area folded graphene formed, as shown in Fig. 1(b). To identify the crystal orientation, we used the T_{LON} method in contact mode, determining the zigzag direction of graphene by comparing the T_{LON} signals obtained at various sample rotation angles. In this method, the closer the angle between the ripple and fast scan directions is to the normal, the smaller is the signal difference between the forward and backward scans. However, if the angle between the ripple and fast scan directions is close to 0°, the forward and backward scan signals have opposite signs, allowing accurate determination of the ripple direction. Using the symmetries of the hexagonal structure of graphene, we confirmed the zigzag directions

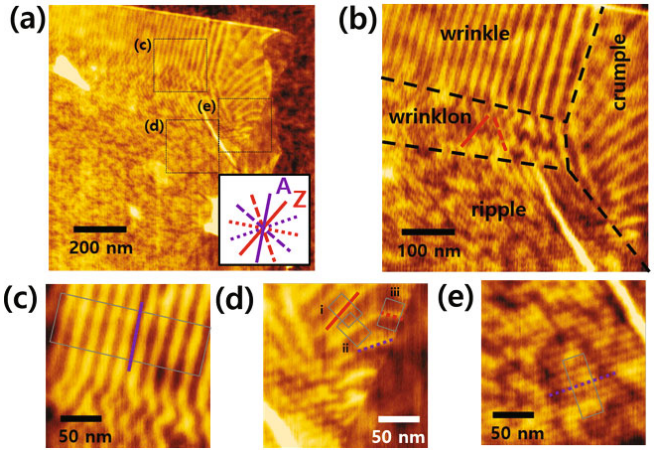

Fig. 4. Strain-induced wrinkle, ripple, and crumple domain formation near the folded area. (a) Magnified topographic image obtained in the red dotted area in Fig. 3(c). The inset shows the zigzag (Z; red lines) and armchair (A; purple lines) directions of TLG. (b) Magnified topographic image showing the wrinkle, ripple, crumple, and wrinklon domains. The black dotted lines indicate the domain boundaries. (c)–(e) Topographic image of the wrinkles, crumples, and ripples. The gray rectangles are the areas considered in the average line profile analysis. The purple and red lines show the corresponding crystal directions designated in the inset of (a).

of the graphene sample through experiments at several rotation angles [8]. We conducted T_{LON} measurements at clockwise-increasing rotation angles of 0°, 36°, and 95°, as shown in Fig. 3(a). The scanned area contains large TLG and SLG regions. The SLG region has three contrast-distinguishable domains and additionally contains a radial domain with six threefold domains. We have previously shown how the zigzag direction identification is useful when finding a radial domain in exfoliated SLG [9]. In this case, the stress normal to the surface forms isotropic radial strains, whereas the ripple formation follows only the zigzag direction of SLG. In the hexagonal lattice, there exist 3 zigzag axes with 60° rotation angles. However, the contrast of the largest domain in the image is uniform. Then, we identify the zigzag direction of the BLG and TLG regions by tracking the folding. Here, deformations and size changes caused by strain were not identified, and there was no relation between the folding angles and hexagonal symmetries such as 30° or 60°, as shown in Fig. 3(b). Then, we switched from the contact mode to DFM mode (also called tapping, dynamic contact, or intermittent contact mode) of the AFM to obtain high-resolution topography images and focused on regions comprising SLG, BLG, TLG, and the SiO_2 substrate. Interestingly, periodic structures were observed near the folding and torn edges, as shown in Fig. 3(c).

After identifying the SLG crystal orientations using the T_{LON} method and tracking the folding process, we could determine the crystal orientations of the TLG region, as shown in the inset of Fig. 4(a). Here, the red and purple lines designate the zigzag (Z) and armchair (A) directions of TLG, respectively. In high-resolution AFM experiments, periodic background signals may appear owing to mechanical vibrations, electrical AC signals caused by incomplete rectification, or external light noise within the position-sensitive photodetector (PSPD) of the AFM. However, the pattern is consistently observed in the whole scanning area even if the scan size is changed. Additionally, we confirmed the observation by imaging wrinkle and ripple domains in TLG in different scan areas, analyzing their amplitude and wavelength. As shown in Fig. 4(b), near the folding edge, we observed domains with 4 types of periodic structures. According to their wavelength and periodicity, we assigned these structures to wrinkles, wrinklons, ripples, and crumples. In this study, wrinkles and ripples are designated as periodic structures; however, wrinkles have distinct wave features that are independent of the topography of the underlying layer, whereas ripples follow it. Wrinklons are a type of wrinkles seen in transition regions where two wrinkles merge or diverge, and crumples are regions where irregular wrinkles seem to have formed by gradual changes in the stress direction. Wrinklons were observed in suspended BLG as well as ordinary hanging curtains, and their wavelength λ follows a simple power law, $\lambda \sim x^m$, where x is the distance to the constrained edge [19]. Wrinklons on metallic thin films on a liquid oil displayed multiple shape transitions near the fluid-solid boundary because of the additional surface energy [20]. However, our wrinklons have a herringbone pattern, similar to that found in compressed thin films on compliant substrates, such as thin metallic films deposited on thick elastomers [21]. The herringbone pattern is known to be caused by an out-of-plane deformation that disperses the biaxial in-plane stresses in all directions. Our wrinklon and crumple structures are located in the transition region between wrinkles and ripples; thus, their formation is attributed to stress relief when surface energy is added. Additionally, wrinklons appear to be formed under a strong surface interaction and biaxial strain, whereas crumples are associated with a relatively weak interaction during a gradual change of the strain direction.

We also related the wrinkles, ripples, and crumples to the zigzag and armchair crystal orientations of TLG. We note that the folded TLG layer is SLG laid on two folded layers, whereas the folded layer in BLG and SLG did not show any periodic structures in topography. Interestingly, most of our periodic structures follow armchair directions. Mechanically exfoliated graphene is known to experience uneven compressive strain because the forces applied when transferring graphene to the substrate are unlikely to be uniform in the entire graphene area [23]. Thus, layer-number-dependent puckering properties were demonstrated in graphene and other 2D materials when they are loosely bound to the substrate

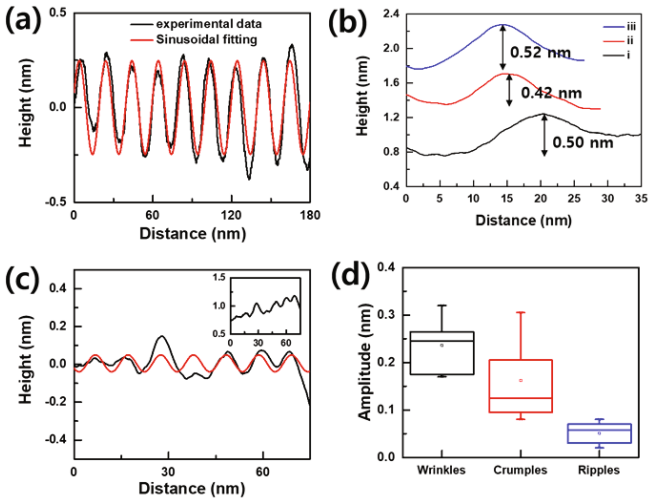

Fig. 5. Average line profile analysis of wrinkles, crumples, and ripples. Average line profiles (black) and simple sinusoidal fitting (red) of the (a) wrinkles and (c) ripples. (b) Average line profiles in the areas designated in Fig. 4(d). (d) Amplitude distribution of individual waves in the wrinkle, crumple, and ripple domains.

[22], and the anisotropic puckering domains of the ripple structure were observed even in exfoliated monolayer graphene [18]. In this case, the ripple (invisible in AFM topography) forms along the zigzag direction of graphene [8]. We suggest that the folding edge acts as a clamping boundary, inducing a strong tensile strain that overcomes the interlayer interaction between the topmost layer and underlying ones. As a result, near the folding edge, a rigid wrinkle forms, starting from the edge and along the armchair direction. Further from the folding edge, the tensile strain is reduced and the transition from wrinkle to ripple occurs, forming a wrinklon. As shown in Fig. 4(b), because the strain direction is distorted, competing biaxial strains are expected. As a result, the wrinklon forms between two zigzag directions of graphene. Contrary to wrinkles and ripples, crumples are regions in which the direction of the tensile strain changes significantly, exhibiting wrinkles in the zigzag and armchair directions rather than exhibiting them aperiodically. We believe that, if the tensile strain dominates, topographically visible periodic structures can form along the armchair direction of graphene.

After classifying the periodic structures near the folded edge of TLG, we investigated their wavelength and amplitude. We extracted the average of line profiles parallel to the reference line for each periodic structure, then fit the data with a simple sinusoidal function. The areas selected for the wrinkles, corrugations, and ripples (Figs. 5(a)–(c), respectively) are designated in Figs. 4(c)–(e). For the ripple structure, the average line profile displayed a slight positive slope (inset of Fig. 5(c)). Because the ripples followed the topography of the underlying surface, as mentioned earlier, the slope needed to be corrected for simplifying the sinusoidal fitting. We used first-order linear correction to flatten the average profile, obtaining the profile shown in Fig. 5(c). Through simple sinusoidal fitting, the wavelengths of wrinkles, corrugations, and ripples are calculated to be 20, ∼20, and 10.38 nm, respectively, and their amplitudes are in the 0.16 – 0.32, 0.07 – 0.3, and 0.01 – 0.07 nm ranges, respectively. Shikai *et al.* categorized the periodic structures of graphene according to their wavelength/width (0.1 – 10 nm, 10 – 100 nm, 100 nm – 1 μm, and above 1 μm) [24]. Because we could not determine the origin of the formation of our structures, we could not use theoretical simulations. However, we can fit our structures to their classification. Accordingly, the periodic structures in our TLG belong to the 0.1 – 10 nm wavelength group, which are those of intrinsic ripples and observed in CVD-grown graphene trenches. A suspended intrinsic ripple exhibited a height of <1 nm [15], and thermally contracted graphene trench on Cu exhibited a wavelength of 0.7 nm and an amplitude of 0.05 nm [25]. CVD-grown graphene on Rh foil displayed ripples having a width and amplitude of 21 – 28 nm and 3.0 – 3.5 nm, respectively [26]. Considering that the periodic structures in our TLG are formed on the third layer over the substrate, the van der Waals interaction with the substrate may be suppressed by the screening of the underlying layers, consistent with the absence of periodic structures on BLG and SLG. Therefore, the wavelength and amplitude may be determined by the competition between the interaction force and tensile strain in the plane.

IV. CONCLUSION

In conclusion, we prepared folded bilayer and trilayer graphene structures induced by weakening the adhesion of mechanically exfoliated SLG to an SiO_2 substrate in high-vacuum conditions. The crystal orientation of SLG, BLG, and TLG was determined by AFM friction anisotropy analysis and by measuring the folding angles. Through high-resolution AFM tapping mode, we observed ripple, wrinkle, and crumple structures. Additionally, we observed herringbone-shaped wrinklon structures, and we suggest that they are induced by competition between the strain distribution and adhesion between graphene and the substrate. Furthermore, the sizes of the structures were compared by computing average line profiles.

ACKNOWLEDGMENTS

This research was supported by Basic Science Research Program through the National Research Foundation of Korea (NRF) funded by the Ministry of Education (NRF-2017R1D1A1B03028169).

REFERENCES

[1] D. Yoon, H. Cheong, J. S. Choi and B. H. Park, J. Korean Phys. Soc. **60**, 1278 (2012).
[2] V. Carozo *et al.*, Nano Lett. **11**, 4527 (2011).
[3] B. Wang *et al.*, Nano Lett. **17**, 1467 (2017).
[4] K. Nagashio *et al.*, J. Appl. Phys. **110**, 024513 (2011).
[5] W. Gao *et al.*, J. Phys. D: Appl. Phys. **47**, 255301 (2014).
[6] J. Annett and G. L. W. Cross, Nature **535**, 271 (2016).
[7] J. S. Choi *et al.*, Rev. Sci. Instrum. **83**, 073905 (2012).
[8] J. S. Choi *et al.*, Sci. Rep. **4**, 7263 (2014).
[9] Y. Park *et al.*, Sci. Rep. **5**, 9390 (2015).
[10] N. D. Mermin, Phys. Rev. **176**, 250 (1968).
[11] D. R. Nelson and L. Peliti, J. Phys. **48**, 1085 (1987).
[12] P. L. Doussal and L. Radzihovsky, Phys. Rev. Lett. **69**, 1209 (1992).
[13] K. S. Novoselov *et al.*, Science **306**, 666 (2004).
[14] K. S. Novoselov *et al.*, Nature **438**, 197 (2005).
[15] J. C. Meyer *et al.*, Nature **446**, 60 (2007).
[16] A. Fasolino, J. H. Los and M. I. Katsnelson, Nat. Mater. **6**, 858 (2007).
[17] K. Xu, P. Cao and J. R. Heath, Nano Lett. **9**, 4446 (2009).
[18] J. S. Choi *et al.*, Science **333**, 607 (2011).
[19] H. Vandeparre *et al.*, Phys. Rev. Lett. **106**, 224301 (2011).
[20] S. Deng and V. Berry, ACS Appl. Mater. Interfaces **8**, 24956 (2016).
[21] X. Chen and J. W. Hutchinson, J. Appl. Mech. **71**, 597 (2004).
[22] C. Lee *et al.*, Science **328**, 76 (2010).
[23] D. Yoon, Y-W. Son and H. Cheong, Nano Lett. **11**, 3227 (2011).
[24] S. Deng and V. Berry, Mater. Today **19**, 197 (2016).
[25] L. Tapasztó *et al.*, Nat. Phys. **8**, 739 (2012).
[26] L. Meng *et al.*, Phys. Rev. B **87**, 205405 (2013).